Probing cell–matrix interactions in RGD-decorated macroporous poly (ethylene glycol) hydrogels for 3D chondrocyte culture

2015 Biomed. Mater. 10 035016

(http://iopscience.iop.org/1748-605X/10/3/035016)

IOP Publishing Biomed. Mater. 10 (2015) 035016 doi:10.1088/1748-6041/10/3/035016

Biomedical Materials

PAPER

RECEIVED
16 January 2015

REVISED
1 May 2015

ACCEPTED FOR PUBLICATION
14 May 2015

PUBLISHED
24 June 2015

Probing cell–matrix interactions in RGD-decorated macroporous poly (ethylene glycol) hydrogels for 3D chondrocyte culture

Jingjing Zhang[1], Ayeesha Mujeeb[1], Yanan Du[2,3], Jianhao Lin[4] and Zigang Ge[1,4]

[1] Department of Biomedical Engineering, College of Engineering, Peking University, Beijing 100871, People's Republic of China
[2] Department of Biomedical Engineering, Tsinghua University, Beijing 100084, People's Republic of China
[3] Collaborative Innovation Center for Diagnosis and Treatment of Infectious Diseases, Hangzhou, 310003, People's Republic of China
[4] Arthritis Clinic and Research Center, Peking University People's Hospital, Beijing, People's Republic of China

E-mail: gez@pku.edu.cn

Keywords: cell adhesion, RGD, macroporous hydrogels

Abstract

Macroporous hydrogels have shown great promise as scaffolds for cartilage engineering by facilitating nutrition transport and tissue in growth. Cell–matrix adhesion—a fundamental process in tissue engineering—has shown a profound effect on subsequent cell phenotype, extracellular matrix (ECM) accumulation, and tissue reorganization. In this study, arginine-glycine-aspartic acid (RGD) was introduced to macroporous hydrogels of poly (ethylene glycol) (PEG) to fabricate PEG-G400 (with 0.4mM RGD) and PEG-G2000 (2mM RGD) to probe the cell–matrix interactions within hydrogels. Primary chondrocytes demonstrated a slightly stretched morphology with increasing RGD concentration and PEG-G2000 hydrogels boosted cell viability, proliferation, and deposition of collagen II and GAG, in comparison to the PEG-G400 and PEG-RED groups. Results also revealed chondrocytes within the cell aggregates underwent dedifferentiation and hypertrophy within RGD incorporated hydrogels, as evidenced by the high level of gene expression of collagen I on day 14 and strong immunohistological staining of collagen X and collagen I on day 35. Evidently, a high concentration of RGD (2mM RGD) enhanced cell–matrix interactions through elevating the expression of integrin β1 and vinculin. Thus, the integration of RGD in macroporous hydrogels with a concentration of 2 mM may be sufficient for improving cell functionality, with a slight probability of dedifferentiation and hypertrophy of chondrocytes.

1. Introduction

Cell–matrix and cell–cell adhesions play an integral role in embryonic development, remodeling, and homeostasis of tissues and organs (DeLise *et al* 2000, Elosegui-Artola *et al* 2014), and are of great importance for cell migration, tissue organization, and differentiation (Tavella *et al* 1997, Anseth *et al* 2008). As most mammalian cells are anchorage-dependent, once encapsulated within a porous material they either adhere to the matrix or other neighboring cells for support (Han *et al* 2014). Cell–matrix and cell–cell adhesions dynamically link the intracellular and extracellular microenvironments through biochemical signals that control cellular functions. An effective technique to enhance cell–matrix adhesions is by modifying the scaffolds with various ECM biomolecules such as gelatin (Chen and Su 2011), collagen, chitosan (Li *et al* 2012, Yang *et al* 2012), and hyaluronic acid (Yoo *et al* 2005, Lebourg *et al* 2014), and short peptides such as the well-studied RGD motif (Jung *et al* 2008, Lee *et al* 2011).

RGD peptide is the most commonly used peptide to improve cell attachment. Compared with other native ECM proteins, RGD is simple, reduces the potential risk of immune reactivity, and can be incorporated into scaffolds in a controlled manner (Bellis 2011). Recently, extensive studies have been performed to assess the effects of RGD on chondrocyte behavior within hydrogel systems. For example, Pluronic®F127 hydrogels with 0.67mM of RGD effectively enhanced viability and proliferation of chondrocytes (Lee *et al* 2011). Similarly, poly(ethylene glycol) (PEG) hydrogels with 0.1–0.4mM of RGD increased the gene expression of collagen I and II of chondrocytes. A dose-dependent inhibitory effect on the redifferentiation of chondrocytes was reported with the incorporation of 0–0.4mM of RGD. In contrast, higher RGD concentrations (0.8mM) did not demonstrate the same results. However, hydrogels with 0.8mM RGD under mechanical loading significantly

enhanced the gene expression of collagen II and the ratio of collagen II/I *in vitro* (Villanueva *et al* 2009).

The above-mentioned studies were performed using traditional hydrogel systems. Most fabricated hydrogels have been shown to contain a homogeneous cell distribution that restricts cell–cell interaction and nutrition exchange, which in turn inhibits chondrogenesis (Zhang 2013, Zhang *et al* 2014) and the accumulation of ECM (Nicodemus *et al* 2011). Recent studies revealed that pore size and pore interconnectivity of scaffolds plays a vital role in cell distribution, maintenance of cell phenotype (Nehrer *et al* 1997), cell proliferation, ECM production (Lien *et al* 2009), tissue infiltration (Rnjak-Kovacina *et al* 2014), and nutrient transport (Zhang 2013). Additionally, a decrease in the pore size leads to cell dedifferentiation (Nehrer *et al* 1997), for example a pore size ranging between 370–400 μm has shown to favor chondrogenic differentiation (Murphy *et al* 2010). Previously, the macroporous hydrogel enhanced the intercellular signaling of human mesenchymal stem cells (Betz *et al* 2010). Therefore, it is necessary to evaluate the function of chondrocytes within 3D macroporous hydrogel systems to serve as a template for cartilage engineering.

In this study, macroporous PEG hydrogels were generated with a freeze-drying/salt-leaching method. Both high and low concentrations (with a concentration of 2mM and 0.4mM, respectively) of RGD were incorporated into macroporous PEG hydrogels. Primary chondrocytes were seeded into PEG hydrogels to explore the effects of cell–matrix adhesions particularly on cell morphology, proliferation, gene expression, and ECM formation. Herein, the relationship between cell adhesion and cell function within 3D macroporous scaffolds is described.

2. Materials and methods

2.1. Synthesis of PEG diacrylate oligomer and fabrication of PEG macroporous hydrogels

Poly (ethylene glycol) diacrylate oligomer (PEGDA) was synthesized according to a previously reported method (Moon *et al* 2009). In brief, dry PEG powder (5 g, 4 kDa, Sigma, USA) was suspended in 80 ml of anhydrous dichloromethane (DCM) (Beijing Tongguang Fine Chemicals, People's Republic of China). A solution containing 1.06 ml of triethylamine (99.7%, Acros Organic, USA) and acryloyl chloride triethylamine (1.26 ml) was added to the reaction mixture drop-wise and left overnight in liquid nitrogen maintained atmospheric temperatures. At room temperature, after washing with 2M K_2CO_3 solution, the mixture was precipitated in cold diethyl ether and freeze-dried at −58 °C for 48 h to obtain lyophilized PEGDA powder. The precursor mixture was prepared by dissolving PEGDA (10% w/v) in a saturated NaCl solution, and was further mixed with NaCl crystals (450 mg ml^{-1}, with a diameter ranging between 80–150 μm) at room temperature. Ammonium persulfate (APS, 0.2 w/v, 25 μl) (Ameresco, People's Republic of China) and *N*,*N*,*N*′,*N*′- tetramethylethylenediamine (TEMED, Sigma, People's Republic of China, 0.5 w/v, 25 μl) were added to crosslink the precursor mixture to fabricate macroporous hydrogels. Hydrogels were immersed in deionized water (DIW) for 48 h before replacing DIW eight times to remove the unreacted precursor and NaCl. The resultant hydrogels were frozen and lyophilized before further use.

2.2. Preparation of RGD-incorporated PEG macroporous hydrogels

The cell adhesion peptide, GGGGRGDS, was conjugated to acrylate PEG-NHS ester (ACLT-PEG3500-NHS, 3500 Da) in $NaHCO_3$ (50mM, pH8.5) for 2 h in the dark. The molar ratio of GGGGRGDS to ACLT-PEG3500-NHS was 1 : 1. The final product was dialyzed in DIW for 24 h. The product, ACLT-PEG-RGD was lyophilized and stored at −80 °C before further use. The same method was used to conjugate GGGGREDS peptide to ACLT-PEG3500-NHS to prepare ACLT-PEG-REG. In addition, PEG hydrogels containing specific concentrations of RED or RGD (0.4mM or 2mM) were prepared by adding to the precursor mixture, as previously described. Therefore, PEG-G2000 (2mM of ACLT-PEG-RGD) and PEG-G400 (0.4mM of ACLT-PEG-RGD) were set up as the experimental groups, whereas PEG-RED (2mM of ACLT-PEG-RED) served as the control group.

2.3. Scanning electron microscopy (SEM) and swelling ratio

The scaffolds were bisected in order to evaluate the surface as well as the cross-section of the scaffolds. The scaffolds were then mounted and sputter coated with gold–palladium. The structure of the scaffolds was examined with scanning electron microscopy (SEM; Quanta 200FEG, FEI, USA) at an accelerating voltage of 5 kV.

The swelling ratio was measured with the following procedure (Nair *et al* 2011). After the weight of the freeze-dried hydrogels was measured, the scaffolds were immersed in phosphate-buffered saline (PBS) at 37 °C for two hours. Any excess water was then removed before measuring the weight of the swollen macroporous hydrogels. The following formula was used to calculate the swelling ratio (ER): $ER = (W_s - W_d)/W_d$, where W_d and W_s are the weight of the dried and swollen scaffolds, respectively.

2.4. Cell culture and cell distribution

Chondrocytes were isolated from the knee joints of pigs (Yorkshire, 10–12 months). The harvested chondrocytes were cultured in Dulbecco's modified Eagle's medium (DMEM) (12800017 Gibco-Invitrogen, People's Republic of China) containing 10% fetal bovine serum, 100 μg ml^{-1} streptomycin, and 100 μg ml^{-1} penicillin. When a sub-confluent cell layer was observed in the cell culture flasks, the cells were trypsinized using 0.05% trypsin-0.53mM EDTA.4Na

(Gibco-Invitrogen, People's Republic of China). The cell pellet was re-suspended in a fresh culture medium to adjust the required cell concentration before seeding into the hydrogels. Prior to the 3 D culture, hydrogels ($4 \times 2.5 \times 1\,mm^3$) were immersed in 75% ethanol for 4 h and washed with PBS before cell seeding. 1 ml of the medium with suspended chondrocytes (3×10^5 cells per well) at passage 2 was added. The culture medium was changed every three days to aid cell growth. Chondrocyte distribution was observed under the optical microscope at 0 h, 4 h and 24 h, respectively.

2.5. Cell viability, F-actin, integrin β1 and vinculin staining

Cell viability was tested by Fluorescein Diacetate (FDA) (F7378 Sigma, People's Republic of China) and propidium iodide (PI) (P4170, Sigma, People's Republic of China) staining. The FDA (100 μl, 2 $\mu g\,ml^{-1}$) solution was added to the samples for 15 min in an incubator at 37 °C. The staining solution was removed and the samples were washed with PBS before adding PI (100 μl, 5 $\mu g\,ml^{-1}$). The samples were then washed with PBS three times for 5 min. The scaffolds were viewed under a confocal laser-scanning microscope (CLSM, LSM510 Zeiss, Germany) at an excitation wavelength of 488 nm (green). As for the F-actin staining, the samples were fixed with 4% paraformaldehyde and the chondrocytes were permeabilized in 0.1% Triton X-100, stained with rhodamine phalloidin (PHDR1, cytoskeleton) for 30 min, followed by nuclear counter staining with 4,6-diamidino-2-phenylindole (DAPI) (Sigma, USA) for 2 h.

For the immunocytochemistry staining of integrin β1, following fixation, the chondrocytes were permeabilized in 0.5% Triton X-100 for 15 min and blocked with 5% BSA for 30 min before washing twice with PBS. Next, the samples were incubated with a rabbit anti-integrin β1 polyclonal antibody (1 : 100 sc-8978, Santa Cruz Biotechnology, Inc, Germany) for 1 h. To remove the non-bound primary antibody, the samples were washed three times with PBS. Subsequently, a secondary antibody (1 : 500 donkey anti-rabbit IgG-Alexa Fluor®-488, bs-0295 d-af488 Bioss, People's Republic of China) was added for 1 h in the dark. To remove the non-bound secondary antibody, the samples were washed five times with PBS. The samples were mounted on glass slides with DAPI and the images were captured using a confocal microscope. For the immunocytochemistry staining of vinculin, the samples were incubated with a vinculin antibody (1 : 1000 sc-5573, Santa Cruz Biotechnology, Inc, Germany) for 1 h followed by secondary antibody staining (1 : 500 donkey anti-rabbit IgG-Alexa Fluor®-488, bs-0295d-af488 Bioss, People's Republic of China) for 1 h. The procedure performed was similar to that of the above-mentioned integrin β1 staining. The samples were visualized using a confocal microscope.

2.6. MTT assay, DNA and GAG quantification

The metabolism of the chondrocytes was measured using MTT assay 3-(4,5-dimethyl-2-thiazolyl)-2, 5-diphenyl-2 H-tetrazolium bromide (M2128 Sigma, People's Republic of China). After culturing for 1, 4 and 7 d, 200 μl of MTT solution was added and the cells were incubated for 3 h before absorbance was detected at 570 nm using a micro-plate reader (Synergy BioTek, USA). The values were recorded after subtracting the data using the blank control (n =4).

The cell numbers were assessed with Hoechst 33258 dye (H6024 Sigma, People's Republic of China). After 14 d in culture, the chondrocytes in each well were lysed with 100μl sterile distilled water and the dissolved solution was transferred into 96-well plates. H33258 solution (100 μl, 0.1 $\mu g\,ml^{-1}$) was added to each well and the readings were recorded in triplicate (where n =3) using a microplate reader (CEMINI XS, Molecular Devices). The fluorescence was recorded at an excitation wavelength of 360 nm and an emission wavelength of 465 nm.

After 14 d in culture, the chondrocytes were digested in proteinase K (50 $\mu g\,ml^{-1}$) at 56 °C overnight and were subsequently examined with 1,9-dimethylmethylene blue (DMMB) (341088, Sigma, People's Republic of China). The solution was vortexed for 30 min, and then centrifuged at 10 000 × g for 10 min. The centrifugal deposits were dissolved in a decomplexation solution and the absorbance was recorded at 630 nm. The standard curve of the sGAG content was recorded with chondroitin sulfate (27042-10 G-F, Sigma, People's Republic of China). The assay was performed in triplicate, where (n =3).

2.7. Real-time-PCR

One milliliter of Trizol (15596-026, Invitrogen) was added to cleave the cells, and the extraction process of the RNA was then carried out according to the manufacturer's instructions. The cDNA was synthesized by following the instructions of the iScript™cDNA synthesis kit (Bio-Rad, CA, USA) after detecting the RNA concentration with the Nano-Drop (Nano-Drop Technologies, DE , USA). The Power SYBR Green PCR Master Mix (Applied Biosystem, CA , USA) was used in this PCR system and the experiment was done on the Applied Biosystems 7500 RT-PCR System (Applied Biosystem) at 95 °C for 15 min, followed by 40 cycles of denaturation for 15 s at 94 °C, 30 s of annealing at 55 °C, and 30 s of elongation at 72 °C. The target genes were normalized by the reference gene glyceraldehydes-3-phosphate dehydrogenase (GAPDH). The primers used in this experiment are listed in table 1.

2.8. Histology and immunohistochemistry staining in vitro

The cell-scaffold constructs were cultured for five weeks. After fixing the constructs in paraformaldehyde solution (4% v/v, pH7.4), the constructs were dehydrated and embedded in paraffin. The constructs were cross-sectioned at a thickness of 5 μm for the staining process. Alcian blue (0.5%, Sigma-Aldrich) in HCl (0.1M) was used for alcian blue staining for 30 min and fast red (Sigma-Aldrich) was used for the nucleus counterstaining. For the immunohistochemistry

staining of collagen I, collagen II and collagen X, the cross-sections were incubated with hydrogen peroxide to block endogenous peroxidase, followed by a pepsin treatment for 20 min. Monoclonal antibodies of collagen I (dilution, 1 : 500), collagen II (dilution, 1 : 500, Clone 6B3; Chemicon Inc), and collagen X (dilustion, 1 : 25) were then added at 4 °C overnight, followed by the addition of a biotinylated goat anti-mouse IgG antibody (Lab Vision Corporation, Fremont, CA, USA). After incubation with streptavidin peroxidase, the slides were stained with 3, 3′-diaminobenzidine as the chromogenic agent. Gill's hematoxylin was applied for the nucleus counterstaining. The final slides were observed under a microscope (DM6000M, Leica, Germany).

2.9. Statistical analysis

The analysis was performed using SPSS V17.0 (one-way ANOVA, LSD, $p < 0.05$). The data are expressed as mean ± standard deviation with significant P values, $^{*}P < 0.05$, $^{**}P < 0.01$, $^{***}P < 0.001$.

3. Results

3.1. Characterization of PEG hydrogels

We developed bioactive PEG macroporous hydrogels using two different concentrations of RGD; 0.4mM and 2mM, respectively. The equilibrium swelling ratio of the modified hydrogels recorded was 12. SEM was performed to study the exterior surface morphologies, and the interior microstructure of the freeze-dried hydrogels. The micrographs indicated conventional interconnected polymer networks with large pores with average diameters of 100 μm (figures 1(a)–(c)). A schematic representation of the RGD integration into the macroporous PEG hydrogels is shown in figure 1(d). The confocal microscopy images in figures 1(e)–(h) indicate the level of RGD integration based on two different concentrations; 0.4 and 2mM. To be able to image the RGD incorporation in PEG hydrogels, fluorescein isothiocyanate conjoined with RGD (FITC-GGGGRGDS) was introduced. An inhomogeneous integration of RGD in the sapatial distribution of both the PEG-G2000 and PEG-G400 groups was observed, with a visibly higher intensity in the PEG-G2000, containing 2 mM RGD (figures 1(f) and (h)). As expected, the micrographs confirmed that chemically cross-linked RGD integration had no effect on the porous microstructures of the hydrogels.

3.2. Role of RGD on cell adhesion, morphology, and viability

The potential role of RGD modified hydrogels as bioactive scaffolds using PEG-G2000 and PEG-G400 was investigated. As a comparison, a RED motif was chosen as a chemical analog to represent the control group; PEG-RED. The cell attachment and morphology were qualitatively assessed by optical microscopy at 0, 4 and 24 h after cell seeding under 3D conditions. The seeded chondrocytes were homogenously distributed within the hydrogels (figures 2(a)–(c)). After 4 h, the cells aggregated to form loose clusters (figures 2(d) and (f)), whereas after 24 h the loose clusters exhibited a more robust spherical shape with average diameters of 50 μm (figures 2(g)–(i)). Additionally, representative cell viability images taken on day 3 revealed a majority of living cells (in green) present inside the RGD-modified hydrogels (figures 2(j)–(l)). No significant difference in cell viability between the three experimental groups was detected.

Table 1. Primer sequences used in RT-PCR analysis.

Target Primer	Sequence forward and reverse (from 5′ to 3′)
GAPDH	ATGGTGAAGGTCGGAGTGAA; AATGAAGGGGTCATTGATGG
Collagen I	CAGAACGGCCTCAGGTACCA; CAGATCACGTCATCGCACAAC
Collagen II	TGAGAGGTCTTCCTGGCAAA; GAAGTCCCTGGAAGCCAGAT
Collagen X	TGCTGCTGCTATTGTCCTTG; TGAAGAACTGTGCCTTGGTG;
SOX-9	ATCAGTACCCGCACCTGCAC; CTTGTAATCCGGGTGGTCCTT
Aggrecan	CATCACCGAGGGTGAAGC; CCAGGGGCAAATGTAAAGG

The chondrocyte morphology and the shape of the cell aggregates was further assessed on day 3, using phalloidin stained F-actin with DAPI. The confocal micrographs revealed well-defined F-actin fibers (in red) around the cell aggregates (figure 3), with varying F-actin fiber arrangements in the three experimental groups. Notably, changes in the F-actin fiber arrangement from the firmly surrounding cell clusters to a multilateral shape, with an increasing RGD concentration were observed (figures 3(a)–(c)). The nuclei of the cells were stained blue with DAPI (figures 3(d)–(f)). Additionally, the representative Z-stack projections of the confocal micrographs (where $n = 5$) were selected to investigate the area of the cell aggregates, the aspect ratio, and the subsequent aggregate roundness. The average values of each category were graphed (figures 3(g)–(i)). The area of the cell aggregates found in the PEG-G2000 groups was nearly 13-fold and 3-fold greater in size in comparison to the cell aggregates in the PEG-RED ($P < 0.001$) and PEG-G400 ($P < 0.001$) hydrogels (figure 3(g)). A significant difference in the aspect ratio of the cell aggregates in PEG-RED and PEG-G2000 ($P < 0.001$) were recorded; however, no significant differences in PEG-G400 and PEG-RED existed (figure 3(h)). Moreover, the roundness of the cell aggregates was significantly lower in the PEG-G2000 groups in comparison to the control group PEG-RED and PEG-G400 ($P < 0.001$) (figure 3(i)). The relatively greater cell area and aspect ratio, and lower roundness of the cell aggregates in the PEG-G2000 hydrogels indicated that the

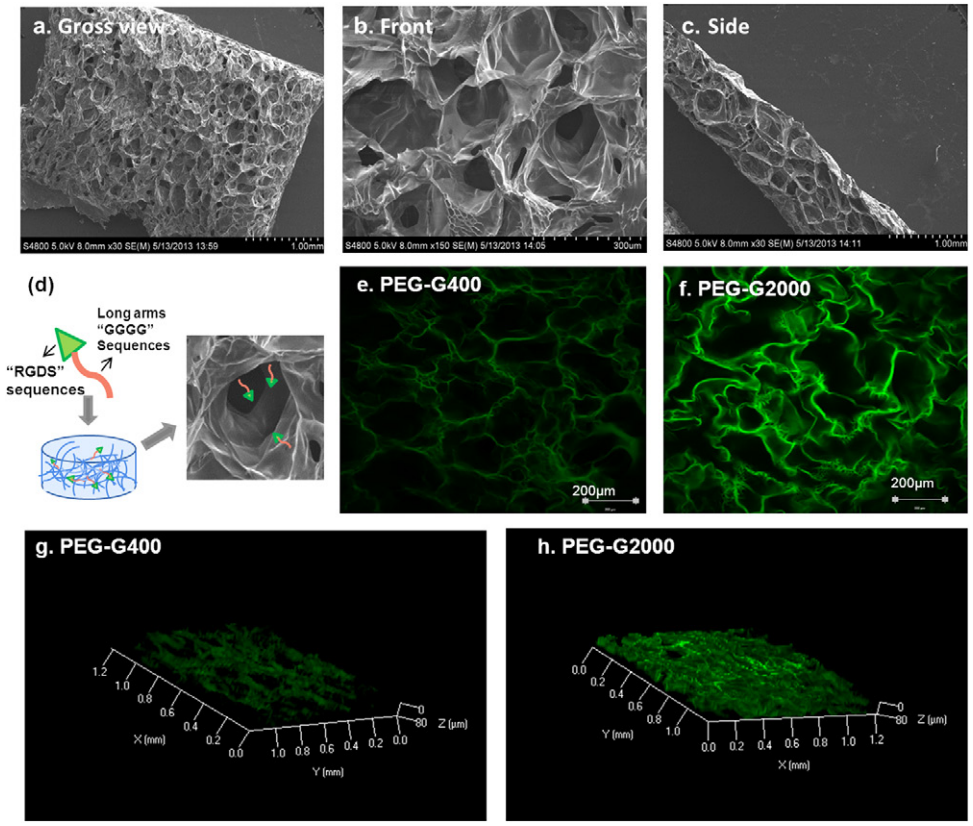

Figure 1. SEM Microphotographs of macro-porous PEG hydrogels. (a) Gross view, (b) front view, (c) side view. Images reveal large pores of ~200 μm. Scale bar = 1 mm and 300 μm. (d) Schematic representation of RGD integration in macroporous PEG hydrogels, (e)–(h) RGD distribution inside hydrogels under confocal microscopy observation with fluorescein isothiocyanate, conjoined with RGD (FITC-GGGGRGDS). Scale bar represents 200 μm.

chondrocytes elongated to form a cytoskeleton. Representative images taken on day 3 (figure 4) revealed that with an increasing RGD concentration, strong integrin β1 staining intensities were found in both the PEG-G400 and PEG-G2000 groups, in comparison to the control group. Strong staining intensities in the RGD-modified hydrogels correlated with the high affinity interactions between the cells and the matrix. This was further confirmed by vinculin staining, as shown in figure 5. The micrographs revealed that the PEG-2000 hydrogels exhibited higher levels of vinculin staining in comparison to the PEG-G400 and the PEG-RED control groups.

3.3. Cell proliferation and GAG quantification

The MTT assay revealed an exponential increase in cell metabolic activity between day 1 and 4 in the culture (figure 6(a)). This phenomenon persisted until day 7, particularly in PEG-G2000, with a significant 1.38-fold increase ($P < 0.05$) in comparison with the PEG-RED control groups. On day 7, no significant increase in cell metabolic activity in the PEG-G400 experimental groups was detected in comparison to the control group. Additionally, on day 14 the cell numbers were recorded in terms of total DNA content using Hoechst 33258 dye (figure 6(b)). The DNA assay shows a significant 2.6-fold increase ($P < 0.01$) in cell numbers in PEG-G2000, in comparison to the PEG-RED group. As a major ECM component of cartilage, GAG is an indicator of neo-cartilage formation. The total GAG content was measured on day 14 via the DMMB assay. The GAG production in the PEG-G2000 groups was approximately 1.08-fold greater in comparison with the other groups ($P < 0.05$). According to figure 6(c) the total GAG content in the PEG-G2000 groups was significantly higher than the other two groups; however, when the results were normalized to GAG per cell number, the values dropped in comparison to PEG-400 and PEG-RED (figure 6(d)). The results demonstrated that the cells produced fewer GAG molecules in PEG-G2000 due to active cell proliferation; however, the overall GAG content produced in PEG-G2000 was evidently higher in comparison with the other two groups. No significant difference in GAG content was found between the PEG-RED and PEG-G400 groups (figure 6(c)), respectively.

3.4. Quantitative gene expression analysis

On day 14, the gene expression of collagen II was higher in the PEG-G2000 scaffolds, with a significant 2.05-fold increase in comparison to PEG-G400 ($P < 0.001$) and PEG-RED ($P < 0.001$). However, no significant difference in the collagen II gene expression was recorded between the PEG-G400 and PEG-RED groups (figure 7). Interestingly, the gene

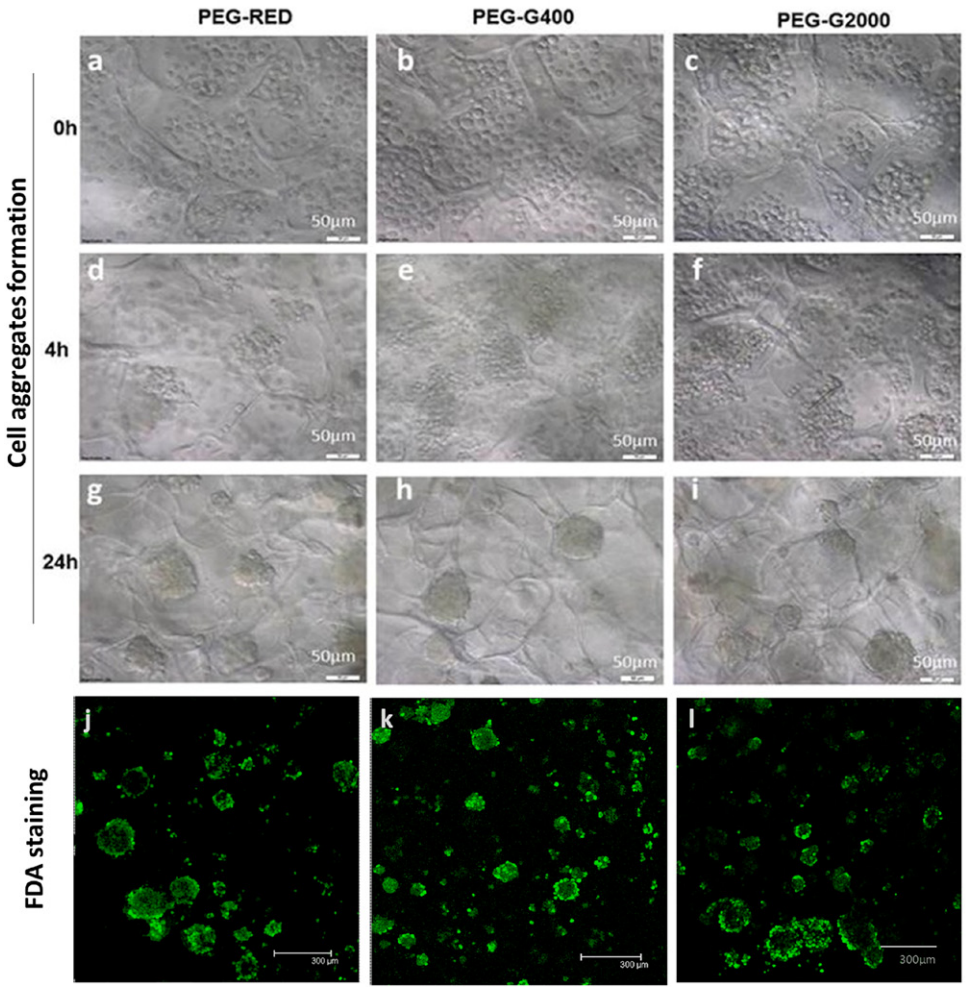

Figure 2. Chondrocyte viability and morphology in 3D culture. Optical microscopy images suggesting the aggregation of the chondrocytes at 0, 4 and 24 h after cell seeding in (a)–(c) PEG-RED, (d)–(f) PEG-G400 and (g)–(i) PEG-G2000. The scale bar represents 50 μm. FDA staining results after 3 d in the culture (j)–(l); the green spots indicating living cells (in green) present. The scale bar represents 300 μm.

expression of aggrecan was up-regulated significantly, with increasing RGD concentration. Approximately a 2-fold increase in aggrecan gene expression in PEG-G400, and an enormous 10-fold increase in the PEG-G2000 groups was recorded. Evidently, a significant difference in the level of aggrecan expression between the PEG-G400 and PEG-G2000 ($P < 0.05$), and PEG-G2000 and PEG-RED ($P < 0.01$) groups was calculated. Moreover, a 7.9-fold increase in collagen I gene expression was also detected in the PEG-G2000 scaffolds, in comparison with PEG-G400 ($P < 0.001$) and PEG-RED ($P < 0.001$); however, no significant difference in collagen I gene expression was found between the PEG-RED and PEG-G400 groups. Likewise, on day 14 no significant difference in the gene expressions of the sox-9 and collagen X were found in all the experimental groups.

3.5. Immunohistochemical examination of tissue-engineered scaffolds

The next challenge was to investigate the effect of RGD incorporation on matrix deposition by chondrocytes *in vitro*. After 35 d in culture, samples were collected and stained with alcian blue and nuclear fast red to assess the GAG deposition, whereas the collagen I, II and X deposition was evaluated through immunohistochemistry staining, respectively. The images presented in figure 8 reveal that the GAG content was limited within the cell aggregates in both the PEG-RED and PEG-G400 hydrogels. However, in the PEG-G2000 hydrogels, GAG molecules were detected both inside and outside the cell aggregates (figures 8(c) and (f)). Additionally, the deposition of collagen I, II and X was predominantly visible inside the PEG-G400 and PEG-G2000 hydrogels, in comparison with the PEG-RED groups (figure 9).

4. Discussion

In this study, high and low concentrations of RGD were incorporated into macroporous PEG hydrogels to investigate cell–matrix interactions *in vitro*. The chondrocytes encapsulated within the PEG-G2000 groups exhibited significantly higher levels of cell proliferation, with enhanced gene expression of collagen I, II and aggrecan, in comparison with the PEG-G400

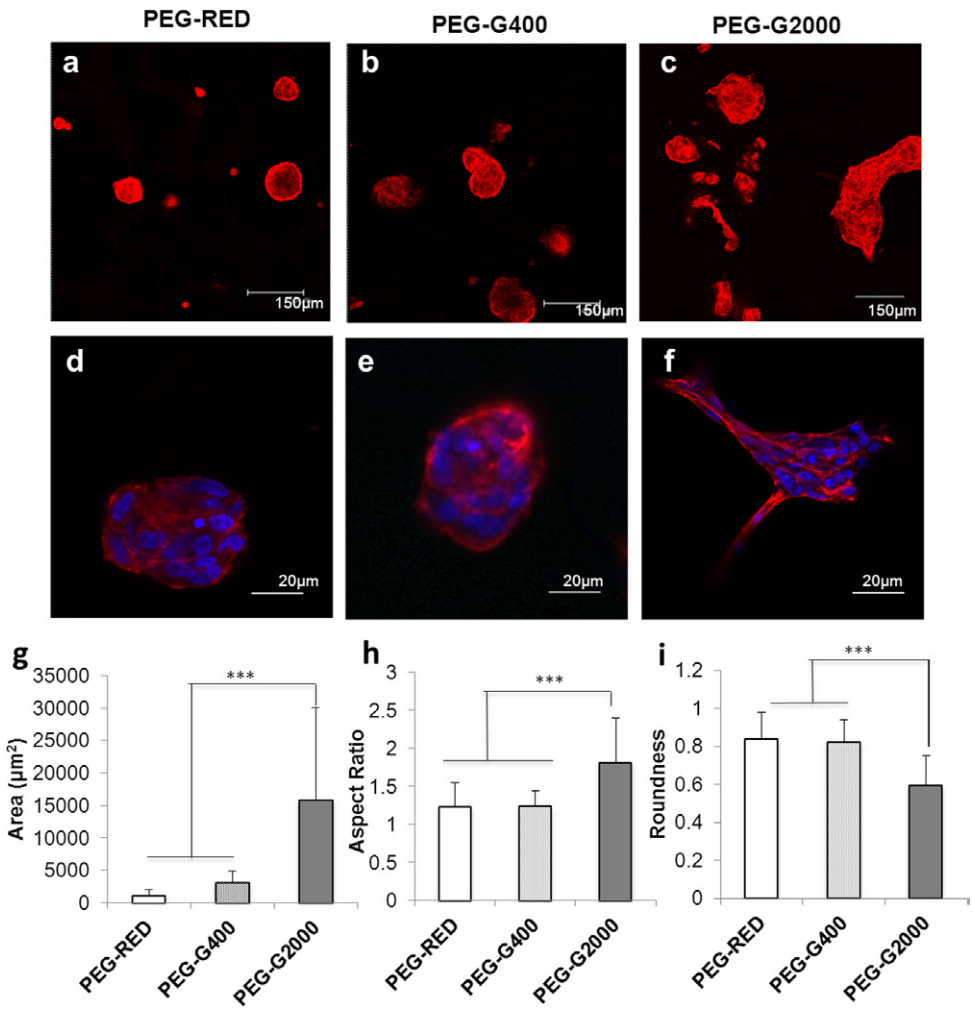

Figure 3. F-actin staining using rhodamine phalloidin with DAPI of chondrocytes within macroporous hydrogels after 3 d in the culture. The nuclei of the cells were stained blue with DAPI and red with F-actin stain. (a), (d) PEG-RED, (b), (e) PEG-G400 and (c), (f) PEG-G2000. (a), (b), (c) Rhodamine phalloidin staining alone and (d), (e), (f) Rhodamine phalloidin with DAPI. The morphology of the cell aggregates was quantified for (g) area, (h) aspect ratio, and (i) roundness. The confocal z-stack projections of the Alexa Fluor 546 phalloidin-stained cells were used for analysis. The error bar represents mean values ± SD (n =5), ***$P < 0.001$.

groups on day 14, but the chondrocytes within the cell aggregates underwent dedifferentiation and hypertrophy within the RGD incorporated hydrogels, as evidenced by the production of collagen X and collagen I on day 35. The concentration of RGD significantly affected the morphology of the chondrocytes. The RGD concentration (greater than 1mM) was sufficient to enable the clustering of focal adhesions and the constriction of actin fibers, which in turn strengthened the adhesive forces (Kambe *et al* 2010). It was reported that 1fmol RGD cm^{-2} may be enough for cell spreading (nascent adhesions) and 10fmol RGD cm^{-2} for the further formation of focal adhesion (mature adhesion), although an optimal RGD concentration would vary for different cells or substrate types (Massia and Hubbell 1991). In this study, the concentration of 0.4mM and 2mM of RGD corresponds to .268–0.28pmol RGD cm^{-2} and 1.34–1.4pmol RGD cm^{-2} (Munger and Sheppard 2011), which was sufficient for chondrocyte attachment. Higher RGD concentrations produced significantly higher adhesive forces per unit area of a single chondrocyte (Kambe *et al* 2010), which was necessary for the cells to perceive the information from the surrounding environment and adapt simultaneously. Additionally, a higher RGD concentration promoted RGD clustering to enhance the bioactivity of the scaffolds. Recent studies have shown that the clustering arrangement of RGD ligands in comparison with RGD alone can enhance cell proliferation (Jiang *et al* 2013). An increase in cell numbers was observed to exhibit stress fibers on the hydrogel surfaces containing RGD clusters of higher ligand density (Gargi Maheshwar *et al* 2000). In addition to the amount of peptide present on the surface, the RGD spacing where the peptide maintains a certain minimum spacing is considered crucial for improving the cell attachment. Relatively small RGD nanospacing (high concentration) induces a strong focal adhesion and a distinct cytoskeleton, and large RGD nanospacing (low concentration) leads to a weak focal adhesion and an indistinct cytoskeleton. RGD nanospacing can also dictate cell lineage differentiation into osteogenic or adipogenic differentiation (Wang *et al* 2013).

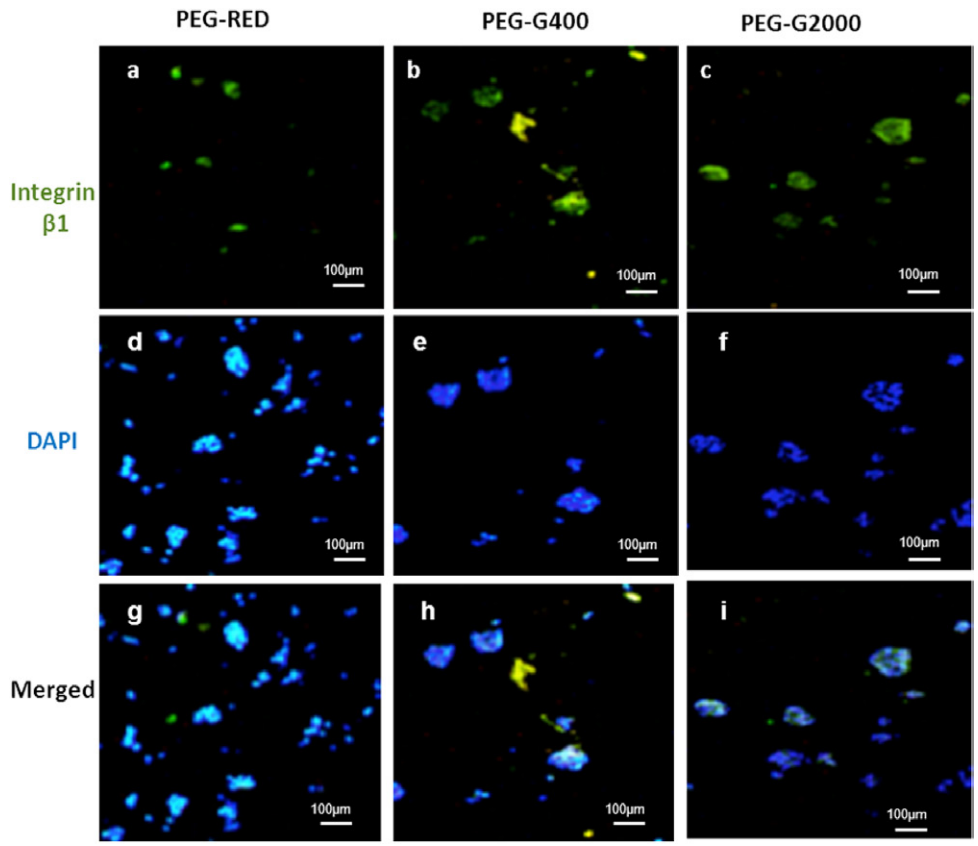

Figure 4. Immunofluorescence images of Integrin β1 of chondrocytes at day 3 in (a), (d), (g) PEG-RED control group, (b), (e), (h) PEG-G400 and (c), (f), (i) PEG-G2000; integrin β1 staining (in green) and the nuclei of the cells stained with DAPI (in blue). Higher expression of integrin β1 was observed in PEG-G2000 than other two groups. Scale bar represents 200 μm.

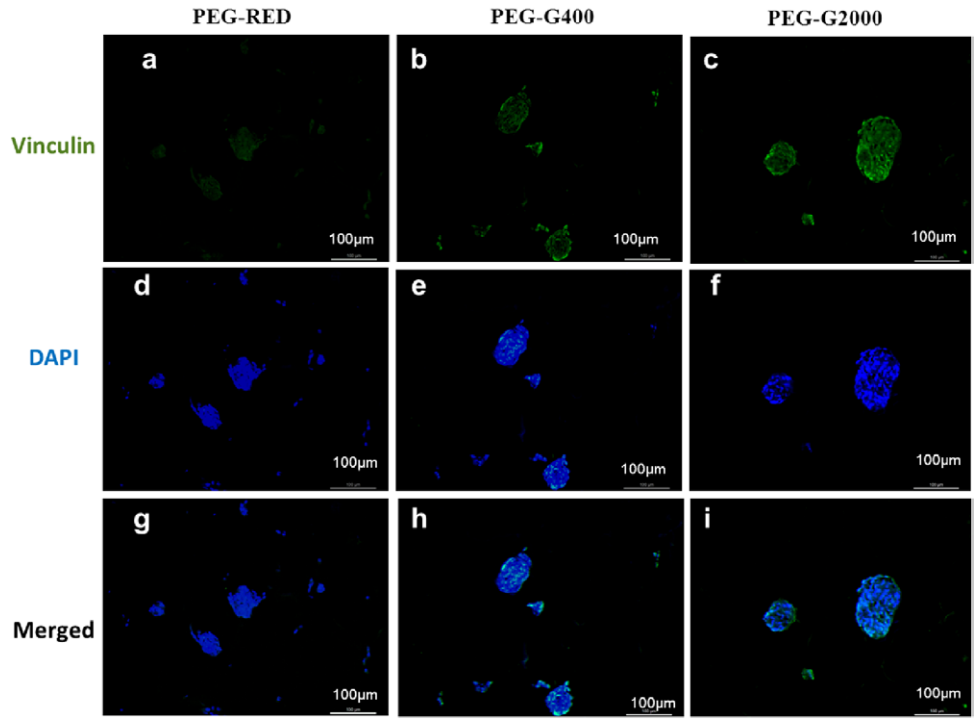

Figure 5. Immunocytochemistry staining for vinculin at day 3 in culture. (a), (d), (g) PEG-RED control group; (b), (e), (h) PEG-G400 and (c), (f), (i) PEG-G2000. Vinculin staining (in green) and the nuclei of cells stained with DAPI (in blue). Higher RGD concentration (2mM) was related to stronger vinculin staining. Scale bar represents 100 μm.

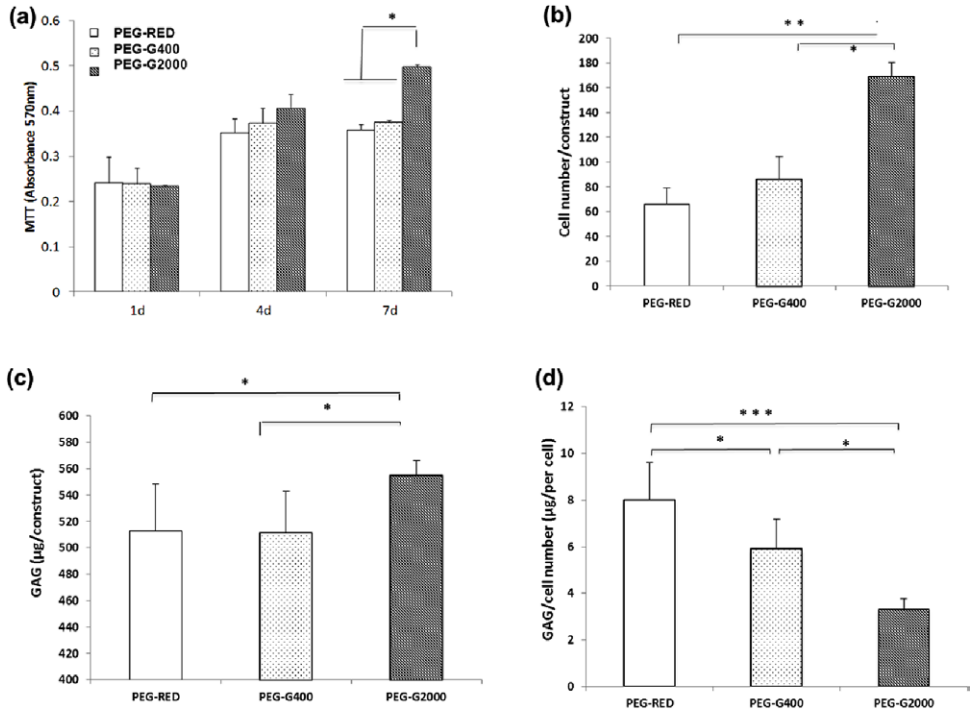

Figure 6. Cell proliferation and GAG quantification. (a) MTT assay for assessing cell metabolic activity on day 1, 4 and 7 in the culture. An exponential increase in metabolic activity was recorded in all three samples, with a relatively significant increase in cell activity in PEG-G2000 on day 7. The data are expressed as mean ± SD (n =4), *P < 0.05. (b) Cell numbers detected by DNA assay on day 14 in the culture. A significant increase in DNA content (corresponding to cell numbers) was measured in the PEG-G2000 scaffolds, in comparison to the PEG-G400 and PEG-RED (control group). The data are expressed as mean ± SD (n =3) *P < 0.05, **P < 0.01. (c) Total GAG content in all three experimental groups on day 14 in the culture. Elevated levels of GAG content in PEG-G2000 were recorded. The data are expressed as mean ± SD (n =3), *P < 0.05. (d) GAG normalized to the cell number, the GAG/cell number dropped significantly in PEG-G2000. The data are expressed as mean ± SD (n =3), *P < 0.05, ***P < 0.001.

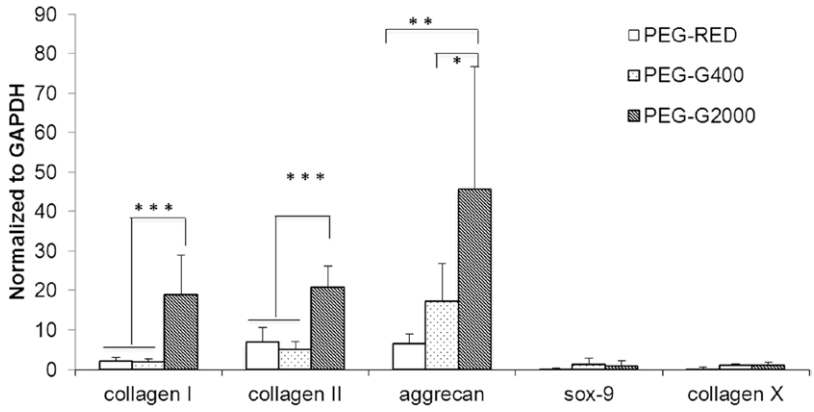

Figure 7. Gene expression levels of collagen I, II, X, aggrecan and, sox-9 measured on 14 d in culture. A significant increase in collagen I, II, and aggrecan gene expression was recorded in the PEG-G2000 hydrogels, in comparison with the other groups. The data are expressed as mean ± SD (n =3), *P < 0.05, **P < 0.01, ***P < 0.001.

The cell–matrix adhesion mediated by RGD acted as vital information processing centers that enabled the cells to sense the rigidity of the scaffolds. And this process was realized through regulating the expression of integrin on the cell membrane (Elosegui-Artola *et al* 2014). This rigidity sensing and adaptation emerges naturally from integrin-ECM bond dynamics, which was demonstrated to determine cell proliferation, cell phenotypes, and even MSC differentiation (Engler *et al* 2006, Martino *et al* 2011). Integrin β1 was reported to mediate the force transduction (Lee *et al* 2004, Cai *et al* 2009). Understanding the dynamics of integrins within focal adhesions was necessary to evaluate the adaptability of the cells to focal adhesions in response to the changes in force (Arjonen *et al* 2012). Recent studies have revealed that the local clustering of ligand-bound integrins, rather than the density of integrins, is paramount for efficient signal transduction (Arnold *et al* 2004). Vinculin has also been shown to regulate integrin binding and clustering, which results in the enlargement of focal adhesions (Humphries *et al* 2007). It was hypothesized that the strong integrin β1 and vinculin

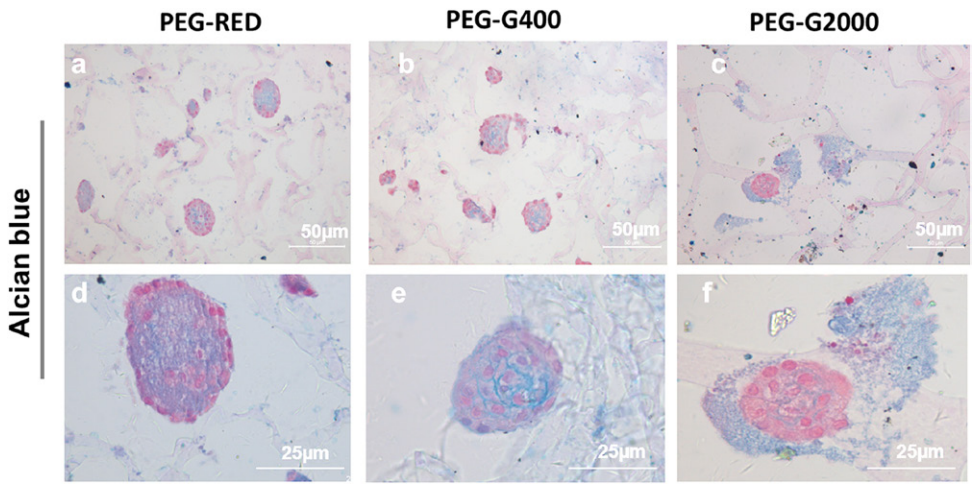

Figure 8. Histological assessment of the chondrocytes embedded in 3D constructs on day 35 in the culture. (a)–(f) Alcian blue and fast red staining micrographs, showing the deposition of the GAG molecules within the cell aggregates present inside the PEG-RED and PEG-G400 scaffolds.

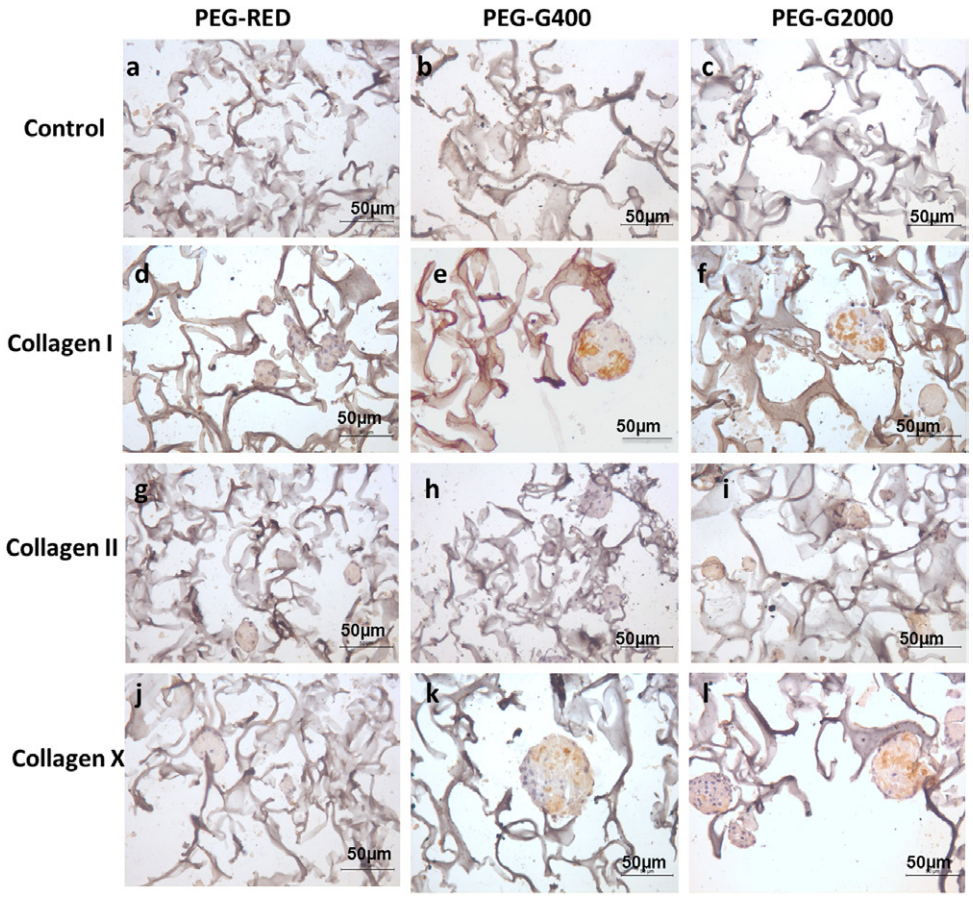

Figure 9. Immunohistochemistry staining of collagen I, II and X. The micrographs demonstrate the accumulation of molecules within the cell aggregates within the 3D matrices. It was difficult to visualize any difference in collagen I, and X accumulation between the PEG-G400 and PEG-G2000 groups; however, a difference in collagen II accumulation was visible between the two groups. PEG-RED served as the control group. The scale bar represents 50 μm and 25 μm, respectively.

staining shown in this study with increasing RGD concentration may be due to focal adhesion enlargement, leading to the formation of multi-lateral morphology of the cell aggregates in PEG-G2000 hydrogels (Wang *et al* 2013). The RGD incorporation significantly influenced the cell phenotypes through altering cell–matrix and cell–cell adhesion. The spread morphology and organized actin cytoskeleton promoted the entry into the cell cycle (Lima *et al* 2007, Margadant 2007). This transition into a proliferative state may be associated with integrin β1, which in turn mediated the coupling of the cytoskeleton to the extracellular matrix. The

activation of integrin enhanced cell proliferation, whereas blocking the integrin β1 inhibited cell proliferation (Enomoto-Iwamoto *et al* 1997). However, this happens when concentrations of RGD are higher than a certain threshold. This is also consistent with our research findings; a higher expression of integrin β1 and vinculin staining was associated with a significant improvement in proliferation.

The heterogeneity was not only observed in cellular morphology within the cell aggregates (figure 4), but also in the extracellular matrix accumulation such as collagen I, II and X within the cell aggregates, as evidenced by immunohistochemistry staining (figure 9). The heterogeneity of the cellular morphology within the cell aggregates may be caused by the inhomogeneous spatial distribution of RGD (figure 1). The inhomogeneous RGD clustering induced an inhomogeneous expression of integrin and further vinculin interactions with talin clustered integrins in an active conformation leading to focal adhesion growth (Ohmori *et al* 2010). This process led to the extension of F-actin in PEG-G2000 as the vinculin anchored F-actin to the cell membranes. This may have been the cause of the irregular morphology of the cell aggregates within the PEG-G2000 group. Also the heterogeneity of the cellular morphology within the cell aggregates led to the heterogeneity in subsequent ECM accumulation. The heterogeneous morphology of the cell aggregates also explains the high standard deviation in the mRNA analysis in the PEG-G2000 samples. Furthermore, the enhanced adhesion of chondrocytes to the scaffold also reduced the immediate cell aggregation, and promoted the extended morphology of the chondrocytes to allow better accessibility to nutrients. The same effect of promoting cell adhesion and prohibiting any immediate matrix-induced cell aggregation was observed in the other RGD modified scaffolds (Re'em *et al* 2010).

In summary, macroporous hydrogels of PEG promoted cell–cell interaction, as evidenced by the extensive formation of cell aggregates. RGD promoted cartilage tissue engineering by enhancing the cell proliferation, GAG synthesis, and the gene expression of aggrecan and collagen II. However, a significant difference was only observed in the PEG-G2000 group, which indicates that there may be a threshold concentration of RGD used to enhance chondrocyte function *in vitro*. Furthermore, the chondrocytes within the cell aggregates underwent dedifferentiation and hypertrophy within the RGD incorporated hydrogels, as evidenced by the high level of gene expression of collagen I on day 14 (figure 7) and the strong immunohistological staining of collagen X and collagen I on day 35 (figure 9). However, the optimal concentration of RGD to promote cartilage tissue engineering applications needs further exploration and the technology for spatially patterning the RGD sequences in 3D scaffolds is still in its initial stages. In the future, dynamic compressive strains should be introduced to investigate the role of cell–matrix adhesion in mechanotransduction for cartilage tissue engineering.

5. Conclusion

In this study, a 3D model of macroporous hydrogels with RGD incorporation was successfully created to investigate the cell–matrix interactions of chondrocytes *in vitro*. Upon integrating RGD at specific concentrations of 0.4 and 2mM, we were able to distinguish the threshold concentration of RGD required to improve scaffold performance. On day 14 in culture, the enhanced chondrocyte proliferation that led to the biosynthesis of GAG content and the elevated gene expression of aggrecan, collagen I and II was observed in the groups containing 0.4 and 2mM RGD. Interestingly, as the culture period progressed to day 35, the accumulation of collagen II was evidently visible in PEG-G2000 in comparison with the PEG-G400 groups, suggesting the formation of cartilage specific ECM. Moreover, the hypertrophy of the chondrocyte was also observed due to the accumulation of collagen X within the cell aggregates in PEG-G400 and PEG-2000, respectively. Hitherto, we have shown some promising results exploiting the function of RGD in correlation with the chondrocyte activity in macroporous hydrogels. By immobilizing RGD, we can substantially tailor chondrocyte behavior and subsequent tissue growth in a controllable manner.

Acknowledgments

The authors would like to acknowledge support from the National Basic Research Program of China grant (973 Program) (2012CB619100) and the National Natural Science Foundation of China grant (81471800, 81271722). The authors would like to thank Dong Cao for the experiment of immunocytochemistry staining of vinculin.

Disclosure statement

The authors declare that they have no competing interests.

References

Arjonen A, Alanko J, Veltel S and Ivaska J 2012 Distinct recycling of active and inactive B1 integrins *Traffic* **13** 610–25

Arnold M, Cavalcanti-Adam E A, Glass R, Bummel J, Eck W, Kantlehner M, Kessler H and Spatz J P 2004 Activation of integrin function by nanopatterned adhesive interfaces *ChemPhysChem* **5** 383–8

Bellis S L 2011 Advantages of RGD peptides for directing cell association with biomaterials *Biomaterials* **32** 4205–10

Betz M W, Yeatts A B, Richbourg W J, Caccamese J F and Cole D P, Falco E E and Fisher J P 2010 Macroporous hydrogels upregulate osteogenic signal expression and promote bone regeneration *Biomacromolecules* **11** 1160–8

Cai N, Wong C C, Tan S C W, Chan V and Liao K 2009 Temporal effect of functional blocking of β1 integrin on cell adhesion strength under serum depletion *Langmuir* **25** 10939–47

Chen J P and Su C H 2011 Surface modification of electrospun PLLA nanofibers by plasma treatment and cationized gelatin immobilization for cartilage tissue engineering *Acta Biomater.* **7** 234–43

DeLise A M, Fisher L and Tuan R S 2000 Cellular interactions and signaling in cartilage development *Osteoarthritis Cartilage* **8** 309–34

Elosegui-Artola A *et al* 2014 Rigidity sensing and adaptation through regulation of integrin types *Nat. Mater.* **13** 631–7

Engler A J, Sen S, Sweeney H L and Discher D E 2006 Matrix elasticity directs stem cell lineage specification *Cell* **126** 677–89

Enomoto-Iwamoto M, Iwamoto M, Nakashima K, Mukudai Y, Boettiger V, Pacifici M, Kurisu K and Suzuki F 1997 Involvement of a5b1 integrin in matrix interactions and proliferation of chondrocytes. *J. Bone Miner. Res.* **12** 1124–32

Han Q Q, Li C, Liu H F, Heng B C, Wu G and Ge Z G 2014 Dynamic distribution of cells in porous scaffolds during cell loading *J. Med. Biol. Eng.* **34** 130–6

Humphries J D, Wang P, Streuli C, Geiger B, Humphries M J and Ballestrem C 2007 Vinculin controls focal adhesion formation by direct interactions with talin and actin *J. Cell Biol.* **179** 1043–57

Jiang L-Y, Lv B and Luo Y 2013 The effects of an RGD-PAMAM dendrimer conjugate in 3D spheroid culture on cell proliferation, expression and aggregation *Biomaterials* **34** 2665–73

Jung H J, Park K, Kim J J, Lee J H, Han K O and Han D K 2008 Effect of RGD-immobilized dual-pore poly(L-lactic acid) scaffolds on chondrocyte proliferation and extracellular matrix production *Artif. Organs* **32** 981–9

Kambe Y, Takeda Y, Yamamoto K, Kojima K, Tamada Y and Tomita N 2010 Effect of RGDS-expressing fibroin dose on initial adhesive force of a single chondrocyte *Biomed. Mater. Eng.* **20** 309–16

Lebourg M, Martinez-Diaz S, Garcia-Giralt N, Torres-Claramunt R, Ribelles J L, Vila-Canet G and Monllau J C 2014 Cell-free cartilage engineering approach using hyaluronic acid-polycaprolactone scaffolds: a study *in vivo J. Biomater. Appl.* **28** 1304–15

Lee H, Choi B G, Moon H J, Choi J, Park K, Jeong B and Han D K 2011 Chondrocyte 3D-culture in RGD-modified crosslinked hydrogel with temperature-controllable modulus *Macromol. Res.* **20** 106–11

Lee J W, Kim Y H, Park K D, Jee K S, Shin J W and Hahn S B 2004 Importance of integrin b1-mediated cell adhesion on biodegradable polymers under serum depletion in mesenchymal stem cells and chondrocytes *Biomaterials* **25** 1901–9

Li C, Wang L, Yang Z, Kim G, Chen H and Ge Z 2012 A viscoelastic chitosan-modified 3D porous poly(L-lactide-co-epsilon-caprolactone) scaffold for cartilage tissue engineering *J. Biomater. Sci. (Polymer Edn)* **23** 405–24

Lien S M, Ko L Y and Huang T J 2009 Effect of pore size on ECM secretion and cell growth in gelatin scaffold for articular cartilage tissue engineering *Acta Biomater.* **5** 670–9

Lima E G, Bian L, Ng K W, Mauck R L, Byers B A, Tuan R S, Ateshian G A and Hung C T 2007 The beneficial effect of delayed compressive loading on tissue-engineered cartilage constructs cultured with TGF-beta3 *Osteoarthritis Cartilage* **15** 1025–33

Maheshwar G, Brown G, Lauffenburger D A, Wells A and Griffith L G 2000 Cell adhesion and motility depend on nanoscale RGD clustering *J. Cell Sci.* **113** 1677–86

Margadant C, van Opstal A and Boonstra J 2007 Focal adhesion signaling and actin stress fibers are dispensable for progression through the ongoing cell cycle *J. Cell Sci.* **120** 66–76

Massia S P and Hubbell J A 1991 An RGD spacing of 440 nm is sufficient for integrin,av,ß3-mediated fibroblast spreading and 140 nm for focal contact and stress fiber formation *J. Cell Biol.* **114** 1089–100

Moon J J, Hahn M S, Kim I, Nsiah B A and West J L 2009 Micropatterning of poly(ethylene glycol) diacrylate hydrogels with biomolecules to regulate and guide endothelial morphogenesis *Tissue Eng.* A **15** 579–85

Murphy C M, Haugh M G and O'Brien F J 2010 Investigating the effect of mean pore size on cell attachment, proliferation and migration in collagen glycosaminoglycan scaffolds for tissue engineering *Biomaterials* **31** 461–6

Martino M M, Tortelli F, Mochizuki M, Traub S, Ben-David D, Kuhn G A, Müller R, Livne E, Eming S A and Hubbell J A 2011 Engineering the growth factor microenvironment with fibronectin domains to promote wound and bone tissue healing *Sci. Transl. Med.* **3** 100ra189

Munger J S and Sheppard D 2011 Cross talk among TGF-beta signaling pathways, integrins, and the extracellular matrix *Cold Spring Harbor Perspect. Biol.* **3** a005017

Nair S, Remya N S, Remya S and Nair P D 2011 A biodegradable *in situ* injectable hydrogel based on chitosan and oxidized hyaluronic acid for tissue engineering applications *Carbohydrate Polym.* **85** 838–44

Nehrer S, Breinan H A, Ramappa A, Young G, Shortkroff S, Louie L K, Sledge C B, Yannas I V and Spector M 1997 Matrix collagen type and pore size influence behavior of seeded canine chondrocytes *Biomaterials* **18** 769–76

Nicodemus G D, Skaalure S C and Bryant S J 2011 Gel structure has an impact on pericellular and extracellular matrix deposition, which subsequently alters metabolic activities in chondrocyte-laden PEG hydrogels *Acta Biomater.* **7** 492–504

Ohmori T, Kashiwakura Y, Ishiwata A, Madoiwa S, Mimuro J, Honda S, Miyata T and Sakata Y 2010 Vinculin activates inside-out signaling of integrin alphaIIbbeta3 in Chinese hamster ovary cells *Biochem. Biophys. Res. Commun.* **400** 323–8

Re'em T, Tsur-Gang O and Cohen S 2010 The effect of immobilized RGD peptide in macroporous alginate scaffolds on TGFbeta1-induced chondrogenesis of human mesenchymal stem cells *Biomaterials* **31** 6746–55

Rnjak-Kovacina J, Wray L S, Golinski J M and Kaplan D L 2014 Arrayed hollow channels in silk-based scaffolds provide functional outcomes for engineering critically sized tissue constructs *Adv. Funct. Mater.* **24** 2188–96

Salinas C N and Anseth K S 2008 The enhancement of chondrogenic differentiation of human mesenchymal stem cells by enzymatically regulated RGD functionalities *Biomaterials* **29** 2370–7

Tavella S, Bellese G, Castagnola P, Martin I, Piccini D, Doliana R, Colombatti A, Cancedda R and Tacchetti C 1997 Regulated expression of fibronectin, laminin and related integrin receptors during the early chondrocyte differentiation *J. Cell Sci.* **110** 2261–70

Villanueva I, Weigel C A and Bryant S J 2009 Cell–matrix interactions and dynamic mechanical loading influence chondrocyte gene expression and bioactivity in PEG-RGD hydrogels *Acta Biomater.* **5** 2832–46

Wang X, Yan C, Ye K, He Y, Li Z and Ding J 2013 Effect of RGD nanospacing on differentiation of stem cells *Biomaterials* **34** 2865–74

Yang Z, Wu Y, Li C, Zhang T, Zou Y, Hui J H, Ge Z and Lee E H 2012 Improved mesenchymal stem cells attachment and *in vitro* cartilage tissue formation on chitosan-modified poly(L-lactide-co-epsilon-caprolactone) scaffold *Tissue Eng.* A **18** 242–51

Yoo H S, Lee E A, Yoon J J and Park T G 2005 Hyaluronic acid modified biodegradable scaffolds for cartilage tissue engineering *Biomaterials* **26** 1925–33

Zhang J, Wu Y, Thote T, Lee E H, Ge Z and Yang Z 2014 The influence of scaffold microstructure on chondrogenic differentiation of mesenchymal stem cells *Biomed. Mater.* **9** 035011

Zhang J J, Yang Z, Li C, Dou Y, Li Y J, Thote T, Wang D and Ge Z G 2013 Cells behave distinctly within sponges and hydrogels due to differences of internal structure *Tissue Eng.* A **19** 2166–75